

## **B. Development of Materials Analysis Tools for Studying NO<sub>x</sub> Adsorber Catalysts**

*Thomas Watkins, Larry Allard, Doug Blom, Michael Lance, Harry Meyer, and Chaitanya Narula*

*Oak Ridge National Laboratory*

*P.O. Box 2008,*

*Oak Ridge, TN 37831-6064*

*(865) 574-2046; fax: (865) 574-3940; e-mail: watkinstr@ornl.gov*

*DOE Technology Development Area Specialist: Dr. Sidney Diamond*

*(202) 586-8032; fax: (202) 586-1600; e-mail: sid.diamond@ee.doe.gov*

*ORNL Technical Advisor: D. Ray Johnson*

*(865) 576-6832; fax: (865) 574-6098; e-mail: johnsondr@ornl.gov*

---

*Contractor: Oak Ridge National Laboratory, Oak Ridge, Tennessee*

*Contract No.: DE-AC05-00OR22725*

---

### **Objective**

- Produce a quantitative understanding of the process/product interdependence leading to catalyst systems with improved final product quality, resulting in diesel emission levels that meet the 2007 emission requirements.

### **Approach**

- Characterize lab-engine tested samples with X-ray diffraction (XRD), spectroscopy, and microscopy. Correlate findings with Cummins data and experience.

### **Accomplishments**

- Supported continued characterization of new materials from various stages of the catalyst's life cycle.
- Obtained rates of desulfation and activation energies for various catalytic compositions after different periods of aging.
- Continued ex-situ microstructural, microchemical, and crystallographic studies of these new materials in simulated engine environments.

### **Future Direction**

- Evaluate gradient formation on a macro scale of active elements on a catalyst as a function of catalyst history and operating conditions.
  - Evaluate thermal degradation of a No<sub>x</sub> stoichiometric reduction (NSR) catalyst as a function of macroscopic position within the catalyst support brick.
  - Determine the soot and ash distribution as a function of macroscopic position within the NSR catalyst support brick.
-

## **Introduction**

To meet the 2007 emission requirements for diesel exhaust, aftertreatment in diesel engines may be necessary. The technology for 2007 will need to integrate aftertreatment with engine control systems. Currently, no commercial off-the-shelf technologies are available to meet these standards. Consequently, Cummins, Inc., is working to understand the basic science necessary to effectively use these catalyst systems. ORNL is assisting with the materials characterization effort.

Base-metal oxides (BMOs) are major components in current nitrogen oxides ( $\text{NO}_x$ ) adsorber catalysts that Cummins seeks to use in aftertreatment systems that contain  $\text{NO}_x$  adsorber catalysts. Although the function of these adsorbers is to collect surface nitrite/nitrate ( $\text{NO}_x$ ) species, they also collect oxy-sulfur ( $\text{SO}_x$ ) species. Both species are to be released from these surface sites during different regenerations, during which the adsorber BMO is either heated to some critical temperature and/or exposed to a reducing or reactant atmosphere. Sulfur adsorption is unfortunately a form of poisoning of adsorber catalysts and is a major problem that must be resolved for BMO-based emission reduction technologies to become commercially viable.

## **Approach**

In general, the crystal structure, morphology, phase distribution, particle size, and surface species of catalytically active materials supplied by Cummins will be characterized using XRD, Raman spectroscopy, and electron microscopy. These materials will come from all stages of the catalyst's life cycle: raw materials, as-calcined, sulfated, regenerated, etc. Both ORNL and Cummins personnel have participated in this work.

## **Samples**

Briefly, a Cummins catalyst supplier provided "core" samples taken from cordierite "bricks" containing the catalyst along the exhaust path for the following conditions: fresh (unused), degreened (zero desulfation hours), and engine-aged catalysts (>zero desulfation hours). Three main variables were considered with these samples: platinum (Pt) loading (1 or 2 wt %), brick position (1, 2, 3 or 4; 1 most upstream), and desulfation hours (the num-

ber of hours the catalyst system is at the desulfation temperature of  $\sim 500^\circ\text{C}$ ; actual engine time  $\sim 150\%$  of desulfation time). The X-ray and spectroscopy work on these samples was discussed previously.<sup>1</sup> The remainder of the microscopy work for these samples is presented in this report.

New engine-tested brick/core and powder samples were examined in FY 2004. These samples consisted of a series of cores with varied amounts of Pt loading, a sample that had lost performance after numerous desulfations, and a sample loaded with sulfur. The powder samples contained Pt,  $\gamma$ -alumina, and BMOs, such as  $\text{BaCO}_3$ .

## **Results**

### **X-ray**

XRD and neutron powder diffraction (NPD) were employed to aid understanding of the crystalline nature of the samples. For the unfamiliar, the following analogy can be applied: As a fingerprint identifies a person, so a diffraction pattern identifies a crystalline material.

Preliminary NPD was attempted with the idea that phases containing lighter elements, namely the target BMO, could be observed. The washcoat components, cordierite ( $\text{Mg}_2\text{Al}_2\text{Si}_5\text{O}_{18}$ ) and possibly Pt, were identified in brick 3, 2 wt % Pt, 1000 desulfation hours. However, no BMO-containing phases were identified/observed. Given the circumstances under which the data were taken, NPD should be revisited in the future when a more appropriate and optimized instrument is available.

Three phases were observed in the E270-3 samples (composition differs from the sample described in the preceding paragraph) with synchrotron radiation: Pt,  $\gamma$ -alumina (washcoat), and cordierite. The samples varied in Pt content and were run for months at  $500^\circ\text{C}$ , cycled in with hydrogen and no sulfur. XRD indicated that the order of decreasing Pt content was E271 (most), E272, 273, and E270 (least); while the chemisorption indicated E270 (most), E271, 272, and E273 (200, 100, 50, 25  $\text{g}/\text{ft}^3$ , respectively). The crystallite size was effectively  $\sim 34$  nm for all four samples. Two other core samples ("commercial samples") were examined with laboratory XRD: one that lost performance after numerous desulfations (Exp6&7) and one that was "loaded" with sulfur (E358-03).

Washcoat components, cordierite, and Pt were identified in both samples. No sulfur-containing compounds were observed. The crystallite size was 10 and 4 nm for samples Exp6&7 and E358-03, respectively, which is in agreement with the observed loss in catalytic performance. Comparison with prior data<sup>1</sup> suggests that sample Exp6&7 has undergone the equivalent of 150 hours of desulfation at 500°C.

A set of FRESH powders was examined with high-temperature XRD. Samples E362a, E363a, and E364a contain a series of BMOs, respectively, which are reported to be stabilizers for Pt. Pt and  $\gamma$ -alumina were identified by XRD in all of these samples. The high-temperature XRD data for all samples showed Pt coalescence/sintering occurring at temperatures in excess of 450°C (e.g., Figure 1), as evidenced by the breadth narrowing and intensity increase of the (111) and (200) Pt peaks. The high-temperature XRD data for sample E364a (FRESH, BaCO<sub>3</sub>) showed the BaCO<sub>3</sub> decomposing/reacting with the Al<sub>2</sub>O<sub>3</sub> to form a spinel, BaAl<sub>2</sub>O<sub>3</sub> (see Figure 2).

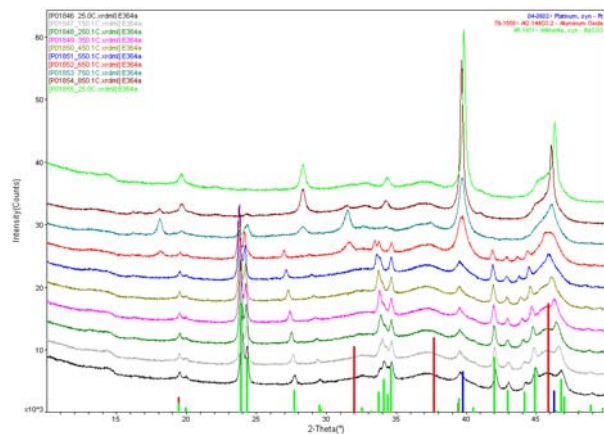


**Figure 1.** The diffraction patterns for E364a as a function of temperature.

## Spectroscopy

Spectroscopic techniques provide important information about the chemical state of and identification of adsorbed surface species. Two complementary spectroscopic techniques are Raman spectroscopy and X-ray photoelectron spectroscopy (XPS), which provide molecular and low-frequency vibrational information, respectively.

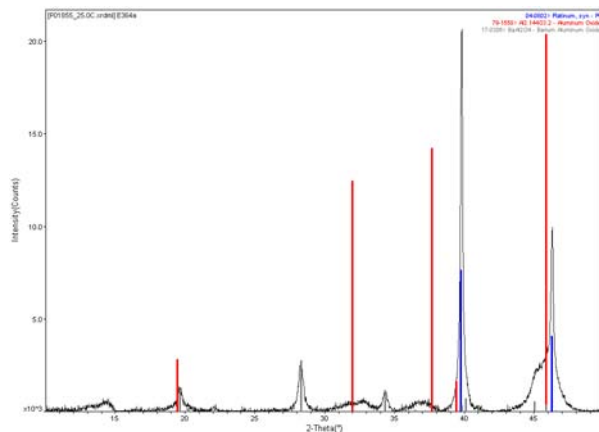


**Figure 2.** The diffraction pattern for E364a after exposure to elevated temperatures.

## Raman

Raman spectroscopy measures the characteristic vibrational energy levels of molecules and crystals and so is very sensitive to any changes in bonding, stoichiometry, and phase/symmetry. In this case, frequency changes of a washcoat component vibration were monitored with desulfation time. Previously, we discovered a decrease in peak width and the increase in peak position of a washcoat-attributed Raman band, which occurs as a result of the growth of the Pt particle size. Although Raman spectroscopy could not directly measure the Pt particle size in these samples, the changes in the Raman spectra with Pt size were calibrated for this specific catalyst formulation so that Raman could nondestructively measure Pt particle coarsening. The origin of the change in Raman spectrum was determined using molecular simulations, as shown in Figure 3. When a Pt atom is adsorbed onto a washcoat particle, the Pt will change the electron charge density by forming a metallic bond with one of the washcoat atoms. This in turn increases the force constants of the washcoat components (see Table 1). Since the bonds are getting stronger, they vibrate at a higher frequency, which explains why the Raman bands increase in frequency with Pt.

Raman spectroscopy is also very sensitive to adsorbed sulfur on the support. The vibration of the SO<sub>4</sub><sup>2-</sup> species has a band at ~960 cm<sup>-1</sup>. Using a high-temperature stage, the amount of sulfur present on a BaO support was monitored in situ in a reducing atmosphere. By monitoring the relative peak heights of BaSO<sub>4</sub>, BaCO<sub>3</sub>, and BaO with

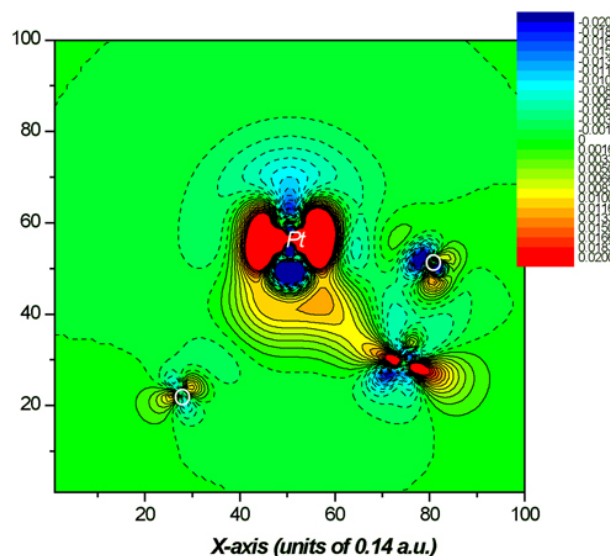


**Figure 3.** The *change* in electron charge distribution that originates from chemical bonding between Pt and the washcoat material. Regions where electrons are withdrawn (blue), and where the charge density is increased (red). The predicted change in force constant describes the observed shift in the Raman spectrum.

**Table 1.** The force constants of a washcoat component before and after Pt adsorption. The K value (in mdyne/Å) generally increases, causing the Raman peaks to shift to higher frequency with Pt concentration

K1(host)	K2(w.Pt)	Site
0.032	0.086	O <sup>1</sup> x
0.093	0.112	O <sup>1</sup> z
0.033	0.038	WC x
0.077	0.113	WC z
0.003	0.005	O <sup>2</sup> x
0.017	0.009	O <sup>2</sup> z

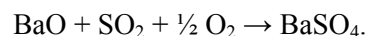
time at different temperatures, the activation energies for sulfation were directly measured. Table 2 shows activation energies for sulfation with and without Pt present and with and without oxygen present. The activation energies for both BaO and BaCO<sub>3</sub> were measured simultaneously since these two phases had peaks in different positions. Three main observations were taken from these results. First, Pt reduces the activation energy in all cases, which is expected. Second, the presence of oxygen reduces the activation energy for sulfation. This suggests that O<sub>2</sub> participates in the formation of BaSO<sub>4</sub> by donating an oxygen atom by the following equations:

**Table 2.** The activation energy of sulfation (kcal/mole) in four conditions, with and without Pt and O<sub>2</sub>. The presence of Pt reduces the activation energy, as does an oxidizing environment

O <sub>2</sub> present?	Pt present?	BaO	BaCO <sub>3</sub>
No	No	17.8	25.4
No	Yes	11.0	17.9
Yes	No	11.6	15.9
Yes	Yes	7.4	13.1



and



However, this means that the reaction can proceed only with O<sub>2</sub> present. Since we have measured sulfation in an anaerobic environment, we believe that the extra oxygen must therefore come from the bulk lattice of the BaO and BaSO<sub>4</sub>. Third, the sulfation of BaO is easier than that of BaCO<sub>3</sub>. These results show the power of Raman spectroscopy for monitoring surface reactions in situ on these catalyst materials. By changing the gaseous environment, we can infer what chemical reactions are taking place and then take steps to improve the catalyst system based on this new information.

### X-ray Photoelectron

XPS was used to analyze chemistry along the length (~5 cm) of individual “troughs” or channels of several “as run” brick/core samples. Figure 4 shows the S 2p, Cl 2p, and Pt 4f core level intensities as a function of position along the catalyst trough of sample E358-03. The sulfur concentration was highest on one end and fell to near-zero intensity by the midpoint of the core. As the sulfur intensity diminished, the chlorine signal grew, reaching a maximum of >1 at. %. Measurements of the Pt 4f core level show a slight decrease at the high-sulfur end, but the overall signal intensity is weak, making the significance of this decrease uncertain. In contrast, the results for sample Exp6&7 showed significant sulfur at only one end of the core, at the position of the first measurement (see Figure 5). Figure 5 also shows that the chlorine intensity was higher in this sample overall and showed an increase from its lowest value at the high-sulfur end of ~2 at. % to a maximum of 5–6

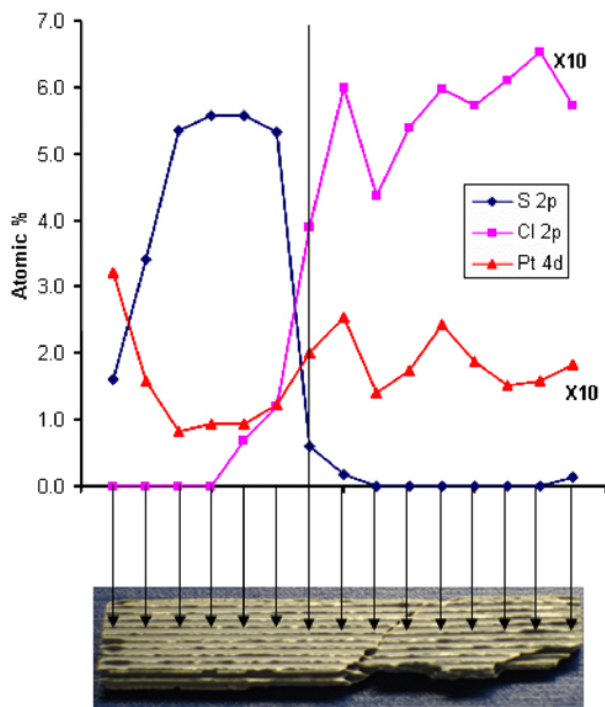


**Figure 4.** S 2p, Cl 2p, and Pt 4f signals as a function of position along a single catalyst trough/channel of sample E358-03. These signal intensities, along with other minor and major component intensities, were used to calculate the at % of each constituent. Measurements were made every  $\sim 5$  mm, as indicated on the photo.

at. % at the opposite end. As with sample E358-03, the Pt showed little variation from one end to the other. A small but significant amount of iron,  $\sim 8$  at. %, was detected on this sample at the sulfur end of the core. This rapidly decreased to  $\sim 2$  at. % by the third measurement location and remained near this level for all other measurements. Taken together, these measurements demonstrated that this measurement technique was helpful in understanding sulfur distribution. The value of this technique was that the measurements were done on real monolith core samples, not samples that were handled or treated specially for ultra-high vacuum surface analytical techniques.

Four brick/core engine-aged samples were desulfated at temperatures of 450, 500, 550 and 600°C and examined using XPS. Figure 6 shows the S 2p core level intensity as a function of position along an individual catalyst channel/ trough for each. There is a definite trend going from 450 to 550 to 600°C. All samples show similar (1.5–2 at. %) and high sulfur at one end versus the other. Each also shows a drop from this initial

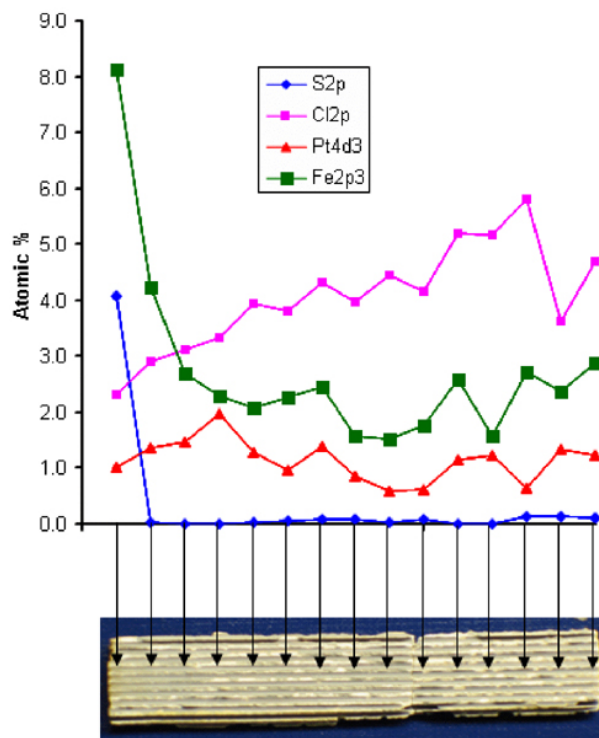


**Figure 5.** S 2p, Cl 2p, Fe 2p and Pt 4f signals as a function of position along a single trough/channel of sample Exp6&7. These signal intensities, along with other minor and major component intensities, were used to calculate the atom % of each constituent. Measurements were made every  $\sim 5$  mm, as indicated on the photo.

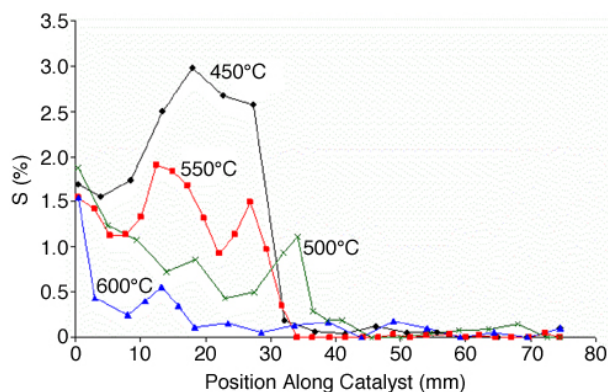


**Figure 6.** Sulfur concentration, as determined by XPS measurements, as a function of position along individual catalyst troughs for samples desulfated at 450, 500, 550, and 600°C. Measurements of the S 2p signal intensity were made every 3–5 mm.

value along the first centimeter of the core. After the initial decrease, all samples show an increase. The length over which the increase occurs varies from 450°C ( $\sim 1.5$  cm) to 550°C ( $\sim 1$  cm) to 600°C ( $\sim 0.5$  cm). The sulfur concentration then de-

creases, reaching near-zero levels by the midpoint of the core. There also appears to be a second, smaller rise for the 450 and 550°C samples at ~3 cm. The 500°C sample showed a similar initial high sulfur level (in fact, the highest of all the samples) but then exhibited a general decrease over the first half of the core before reaching near-zero levels. Two separate trials on two different (but nearly adjacent) troughs showed the 500°C was self-consistent. Further studies should be attempted to determine the reason that this sample did not follow the trend of the others. No significant trends for other minor components were noted. Chlorine levels for the four samples were generally low and did not correlate with the sulfur signal as noted above for sample E358-03. This study showed that tracking the sulfur on real catalyst cores was feasible and showed trends versus desulfation temperature.

### **Microscopy**

Transmission electron microscopy (TEM), scanning transmission electron microscopy (STEM), and electron probe microanalysis (EPMA) techniques were used to continue characterization of the microstructure of the NO<sub>x</sub> trap catalysts. In the previous report, the microstructure and chemistry of samples with 1 wt % Pt loading at different positions along the reactor were studied; and the changes in morphology of Pt particles, as well as the distribution of elements such as the trapping component within the washcoat, were elucidated. In subsequent work, a series of samples with 2 wt % Pt loading were studied in like fashion. Some example results and main conclusions from the microscopy and microprobe experiments are given below.

In contrast to the 1 wt % Pt loading results, high-resolution bright-field TEM images of the 2 wt % Pt fresh catalyst did in fact clearly reveal discrete Pt catalyst particles (see Figure 7). Similar results were obtained with high-angle annular dark-field (HA-ADF) images taken in the Hitachi HD-2000 STEM instrument. The de-greened samples showed discrete fine particles of Pt, on the order of 5 nm in diameter, using both TEM and STEM methods. HA-ADF images on the STEM provided a facile method for imaging the particles in high contrast and for measuring particle sizes. These measurements were made on all observed

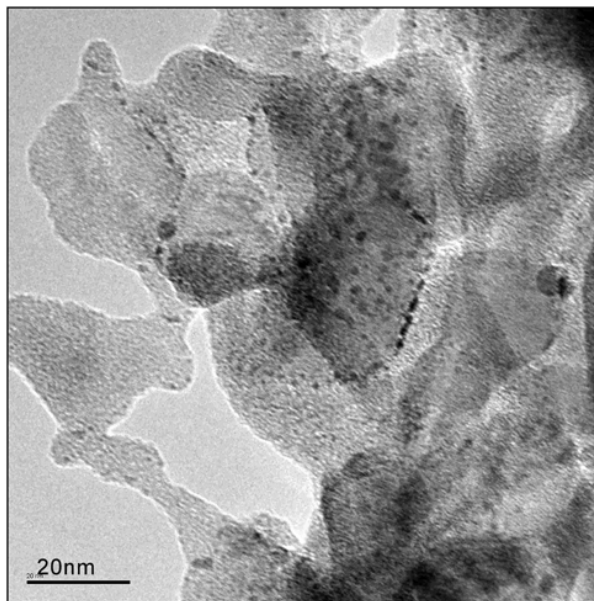


**Figure 7.** Bright-field TEM micrograph of fresh 2 wt % Pt catalyst sample with discrete Pt particles evident in brick 2, FRESH.

samples (except the fresh specimen). Samples from the bricks with 2 wt % Pt loading with 150, 500, and 1000 desulfation hours displayed 8-, 10.5-, and 11.5-nm particles, respectively. Figure 8 shows the HA-ADF image of brick 2 with 150 desulfation hours, for example. The results were nearly identical, with respect to average particle size, to those obtained from the 1 wt % Pt samples, with only a slight increase of about 1 nm in the diameters of particles in the 500 and 1000 desulfation hour samples.

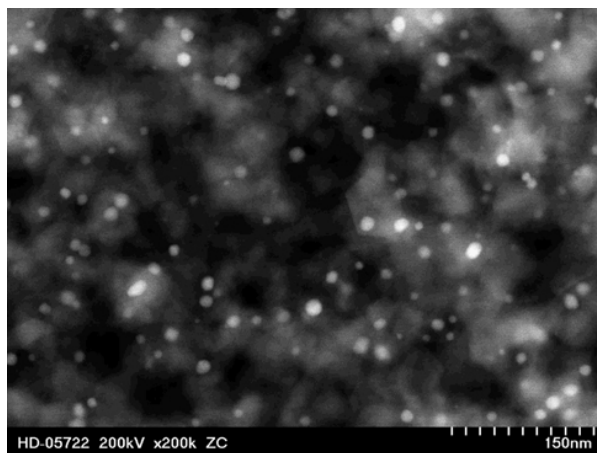


**Figure 8.** Z-contrast STEM image illustrating dispersion and size of 2 wt % Pt particles in brick 2 after 150 hours of deS.

EPMA was used to determine the bulk distributions and quantitative measurements of the Pt trapping component and sulfur species by acquiring X-ray counts from small regions from the outer surface of the washcoat layer into the cordierite framework. These measurements mapped Pt at the 2 wt % level, as expected. The trapping component initially was present also at about the 0.7–0.8 wt % level, and sulfur in all the 2 wt % Pt samples was less than 0.1 wt % in the bulk of the washcoat; but it seemed to concentrate in thin layers at the cordierite-washcoat interface. Unlike the 1 wt % Pt samples, where Pt showed concentrations primarily at free surfaces within and external to the two washcoat layers, Pt was very uniformly dispersed within the washcoats of the 2 wt % Pt samples (see Figure 9). The differences are likely due to different rates of drying employed in deposition of the washcoats on the cordierite support. In the fresh samples, the trapping component was sometimes observed to be strongly concentrated at the interface between the inner washcoat and the cordierite framework material. In most samples, however, the trapping component showed a uniform concentration, with occasional high concentrations in very small, widely scattered regions.

The trapping component concentration remained very uniform throughout the washcoat with engine aging, but the overall concentration decreased by 150 desulfation hours to about the 0.5 wt % level. As with 1 wt % Pt samples, this result is important because it shows the trapping component that is available for NO<sub>x</sub> adsorption, whereas the XRD data showed only total trapping component. Thus the decrease in the total amount of trapping component coupled with the increase in Pt particle size could suggest a reduction in the total number and surface area of Pt-trapping component contact sites upon aging. This would also explain the reduced performance of the NO<sub>x</sub> trap. Energy-dispersion spectroscopy spectra in the TEM showed small trapping component peaks, but no discrete trapping component phase was detected. Platinum particle sizes at brick positions 1 and 4 in 2 wt % Pt loaded samples were similar to those of brick 2, indicating that the particle growth behavior was similar regardless of sample position in the reactor.

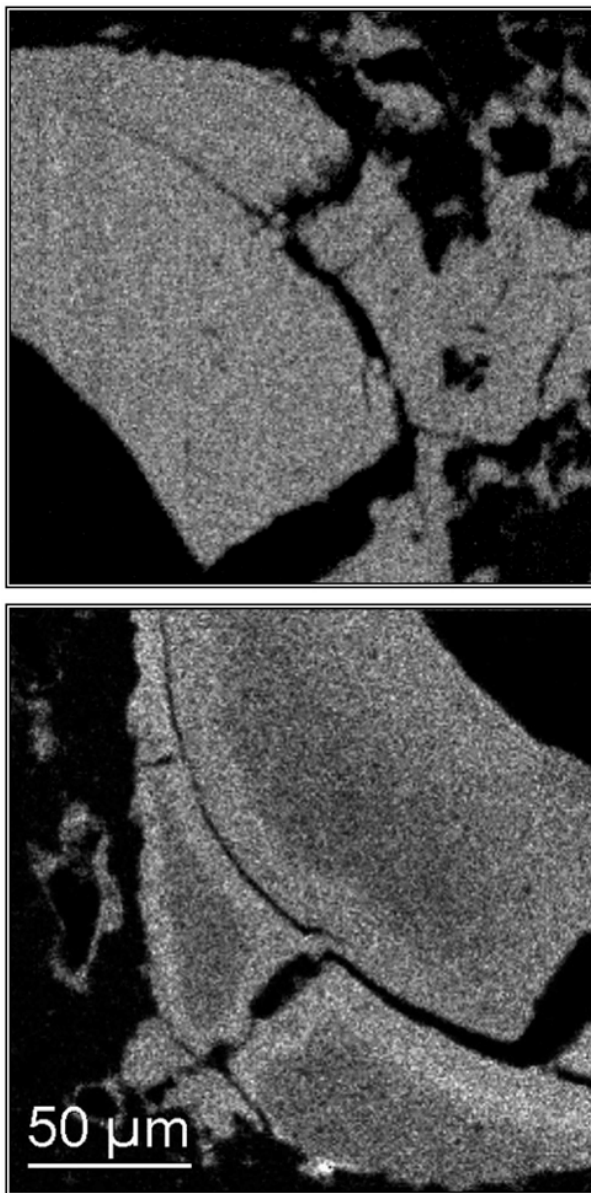


**Figure 9.** Two EPMA Pt X-ray maps demonstrating differences in dispersion of Pt between the (a) 1 wt % Pt and (b) 2 wt % Pt in both bricks after 150 hours of deS. Pt is uniformly distributed in the 2 wt % sample; in the 1 wt % sample, it is higher at the surface and free surfaces throughout the washcoat than in the bulk.

## References

1. Thomas Watkins, Larry Allard, Doug Blom, Michael Lance, Chaitanya Narula, and Harry Meyer, "Development of Materials Analysis Tools for Studying NO<sub>x</sub> Adsorber Catalysts," *Heavy Vehicle Propulsion Materials 2003 Annual Progress Report*, Energy Efficiency and Renew-

able Energy Office of FreedomCAR and Vehicle Technologies, March 2004.

### **Publications**

H. L. Fang and M. J. Lance, "Influence of Soot Surface Changes on DPF Regeneration," accepted for publication in *J. Soc. Auto. Eng.* (2004).

J. Parks, A. Watson, B. Epling, L. Campbell, R. England, N. Currier, A. Yezerets, H. Fang, T. Yonushonis, T. Gallant, T. Watkins, D. Blom, L. Allard, M. Lance, H. Meyer and C. Narula, "NO<sub>x</sub> Absorber Catalyst Durability: Light- and Heavy-Duty Perspectives," pp. 304–311 in *Proceedings of 2003 DEER Conference: 9th Diesel Engine Emission Reduction Conference*, August 24–28, 2003, Newport, RI.

### **Presentations**

T. R. Watkins, L. Allard, D. Blom, M. J. Lance, C. Narula, H. Meyer, R. D. England, H. Fang, and T. Yonushonis, "Development of Materials Analysis Tools for Studying NO<sub>x</sub> Adsorber Catalysts," presented at NLCat 2003, 4th DOE National Laboratory Catalysis Conference, Oak Ridge, Tennessee, October 23, 2003.

T. R. Watkins, L. Allard, D. Blom, M. J. Lance, C. Narula, H. Meyer, R. D. England, H. Fang, and T. Yonushonis, "Development of Materials Analysis Tools for Studying NO<sub>x</sub> Adsorber Catalysts," presented at the 53th Annual Denver Conference, Steamboat Springs, Colorado, August 2, 2004.

T. R. Watkins, L. Allard, D. Blom, M. J. Lance, C. Narula, H. Meyer, R. D. England, H. Fang, and T. Yonushonis, "Development of Materials Analysis Tools for Studying NO<sub>x</sub> Adsorber Catalysts," presented by D. R. Johnson at the 10<sup>th</sup> Diesel Engine Emission Reduction (DEER) Conference, Coronado, California, August 30, 2004.